First-principles prediction of an enhanced optical second-harmonic susceptibility of low-dimensional alkali-metal chalcogenides

Jung-Hwan Song,[1] Arthur J. Freeman,[1,2] Tarun K. Bera,[3] In Chung,[3] and Mercouri G. Kanatzidis[3]
[1]*Department of Physics and Astronomy, Northwestern University, Evanston, Illinois 60208, USA*
[2]*Department of Materials Science and Engineering, Northwestern University, Evanston, Illinois 60208, USA*
[3]*Department of Chemistry, Northwestern University, Evanston, Illinois 60208, USA*
(Received 8 May 2009; published 9 June 2009)

Fully first-principles calculations for the second-harmonic susceptibilities of recently synthesized alkali-metal chalcogenides such as $KPSe_6$, $K_2P_2Se_6$, $LiAsS_2$, and $NaAsSe_2$ predict a record-breaking second-harmonic generation coefficient among materials with band gaps larger than 1.0 eV, with the highest value being that for $NaAsSe_2$, namely, 324.6 pm/V. A detailed analysis of their highly precise full-potential linearized augmented plane-wave electronic structures suggests that it is a quasi-one-dimensional structural anisotropy with a strong covalent character that yields the very large second-harmonic coefficients.

DOI: 10.1103/PhysRevB.79.245203 PACS number(s): 78.20.−e, 42.65.Ky, 42.79.Nv, 78.47.N−

I. INTRODUCTION

Experimental and theoretical studies of nonlinear optical (NLO) properties have been intensively performed especially for second-harmonic generation (SHG) because frequency-doubling conversion creates powerful laser sources possible from the UV (e.g., LiB_3O_5) to the far-IR (e.g., $AgGaSe_2$) region.[1–3] There are however few efficient NLO materials available because applications require large NLO coefficients, a wide optical-transparency energy window, and a phase matching characteristic.[1–4] Currently intense effort is being devoted to obtaining better NLO materials for the optical frequency conversion from the near-infrared to the mid-infrared regions.[5] Recently, new promising NLO materials for IR applications such as the noncentrosymmetric alkali-metal chalcogenides, $KPSe_6$,[6] $K_2P_2Se_6$,[7] $LiAsS_2$,[8] and $NaAsSe_2$,[9] have been found, which demonstrate very large SHG efficiencies compared to the commercially used material, $AgGaSe_2$. For instance, $K_2P_2Se_6$ and $LiAsS_2$ showed 20-fold (at 890 nm) and 10-fold (at 790 nm) higher SHG intensities, respectively, compared to $AgGaSe_2$.[7,8] Importantly, the strong SHG signals manifested in glassy forms of $KPSe_6$ and $K_2P_2Se_6$, without any special treatment such as thermal poling, may have a great impact on telecommunications due to their possible use as infrared optical fibers.[7] However, a theoretical understanding of the very large SHG coefficients for these materials is still lacking. To resolve this, we calculated from first principles the frequency-dependent SHG coefficients and investigated the electronic structures of these materials to find the key NLO/structure property relationships. We find, in $NaAsSe_2$, the highest static SHG coefficient to date, 324.6 pm/V, among known materials with band gaps larger than 1.0 eV. A detailed analysis of this system gives insights for designing better SHG materials: these first-principles calculations reveal that their quasi-one-dimensional character, not present in other commercial SHG materials such as $AgGaSe_2$, plays an important role in the calculated very large SHG coefficients and thus the strong SHG intensities observed in recent experiments.[7,8] These results suggest design principles for obtaining exceptionally good SHG materials, namely, the low-dimensional character of crystal structures with large covalency in the atomic bonds.

II. METHOD

The electronic structures and their optical matrix elements were calculated using the full-potential linearized augmented plane-wave method[10,11] within the local-density approximation (LDA) and the Hedin and Lundqvist exchange and correlation potential.[12] The core states and the valence states were treated fully relativistically and scalar relativistically, respectively. For **k**-space integrations, the numbers of special **k** points in the irreducible Brillouin-zone (BZ) wedge of $KPSe_6$, $K_2P_2Se_6$, $LiAsS_2$, and $NaAsSe_2$ were 12, 12, 38, and 15, respectively. The energy cutoffs for the interstitial plane-wave basis and the star functions were 13.0 and 144.0 Ry, respectively.

We then adopt the so-called length-gauge formalism derived by Sipe and Ghahramani[13] and Aversa and Sipe,[14] which is basically second-order perturbation theory with the interaction between the electromagnetic field in the long-wavelength limit and the materials in terms of $e\vec{r}\cdot\vec{E}$, in which $\vec{r}$ is the position operator and $\vec{E}$ is the electromagnetic field. In this approach, excitonic and local-field effects are ignored.[2] Within the length-gauge formalism, we use expressions for the frequency-dependent SHG coefficients.[15–17] We then obtain the imaginary parts by writing the frequency ω as $\omega+i\delta$ and then taking the limit $\delta\rightarrow 0$. Lastly, the real parts of the SHG coefficients are calculated from the Kramers-Kronig relations (KKRs). For the SHG calculations, integrations over the BZ are done with the special **k**-point method, for which we use a very fine **k**-point mesh: 1700, 1500, 2426, and 2048 irreducible **k** points for $KPSe_6$, $K_2P_2Se_6$, $LiAsS_2$, and $NaAsSe_2$, respectively, due to the low symmetries of the crystal structures and rapidly varying band structures and **k**-space matrix elements. The energy cutoff for SHG calculations is taken to be at least 30 eV above the valence-band maximum (VBM).

III. RESULTS AND DISCUSSIONS

Noncentrosymmetric $KPSe_6$, $K_2P_2Se_6$, $LiAsS_2$, and $NaAsSe_2$ crystallize with orthorhombic $Pca2_1$, trigonal

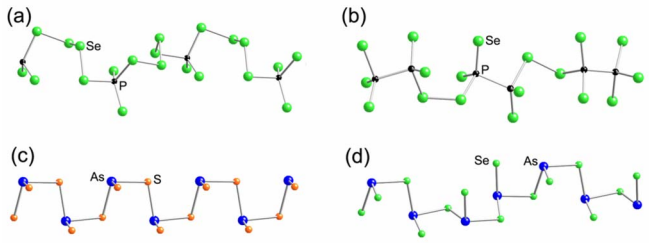

FIG. 1. (Color online) Single-chain structures of (a) $KPSe_6$, (b) $K_2P_2Se_6$, (c) $LiAsS_2$, and (d) $NaAsSe_2$. The alkali-metal atoms are not shown.

$P3_121$, monoclinic Cc, and monoclinic Pc space groups, respectively.[6–9] Each system has infinite quasi-one-dimensional chains of the polymeric species $^1_\infty[PSe_6^{1-}]$, $^1_\infty[P_2Se_6^{2-}]$, $^1_\infty[AsS_2^{1-}]$, and $^1_\infty[AsSe_2^{1-}]$, respectively, which then form three-dimensional crystals mainly through ionic interactions with alkali-metal ions between the chains.[6–9] The repeating units in each chain (e.g., $[AsSe_2^{1-}]$) have mainly two types of chalcogenide atoms: *bridging atoms*, which connect the As atoms between repeat units via covalent As-S-As bonding, and *terminal atoms*, which are covalently bonded with each As atom, as shown in Fig. 1. In the case of $^1_\infty[PSe_6^{1-}]$ and $^1_\infty[P_2Se_6^{2-}]$, the bridging units are polychalcogenide fragments instead of atoms, e.g., P-Se-Se-Se-Se-P and P-Se-Se-P, respectively.

The densities of states of these alkali-metal chalcogenides have common features due to their similar crystal structures, as shown in Fig. 2. Since the energy levels near the band gap are predominantly p orbitals of constituent atoms in the repeat units, the p-p mixing is expected to have a strong effect on their electronic structures. Indeed, the angular momentum-resolved local density of states (LDOS) in Fig. 2 show that the energy levels between approximately −6 and −2.5 eV below the VBM are derived from the strong covalent interactions between P (or As) and mainly bridging S (or Se) p orbitals: the two covalent bonds (Fig. 1) of the bridging S (or Se) have stronger hybridization with their counterpart P (or As) atoms in the repeat units than with the terminal S (or Se). On the other hand, the terminal S (or Se), which has stronger ionic interactions with alkali-metal ions, contributes most to the higher energy levels between −2.5 eV and the VBM.

The well-known LDA underestimation of the band gaps may result in incorrect SHG coefficients since they are more sensitive to the band gaps than the linear-response values due to higher power energy differences in the denominators of the formalism.[16] Moreover, in the static limit, the SHG coefficients show the general trend of having an inverse correlation with the band gaps.[2] To avoid this problem, we take quasiparticle self-energy corrections at the level of scissor operators in which the energy bands are rigidly shifted to have the correct band gap, but the r^a_{nm} and the $r^a_{mn;b}$ matrix elements are kept the same[18] since the Kohn-Sham wave functions are assumed to be close to the true quasiparticle wave functions.

$KPSe_6$, $K_2P_2Se_6$, $LiAsS_2$, and $NaAsSe_2$ have three, one, six, and six nonvanishing independent $\chi^{(2)}$ components in the static limit based on their space groups and the Kleinman symmetry.[19] Their highest components and, for comparison, those calculated for $RbPSe_6$, GaAs, GaP, and $AgGaSe_2$ (the widely used IR SHG material today) are shown in Table I. Note that, due to their high symmetries, GaAs, GaP, and

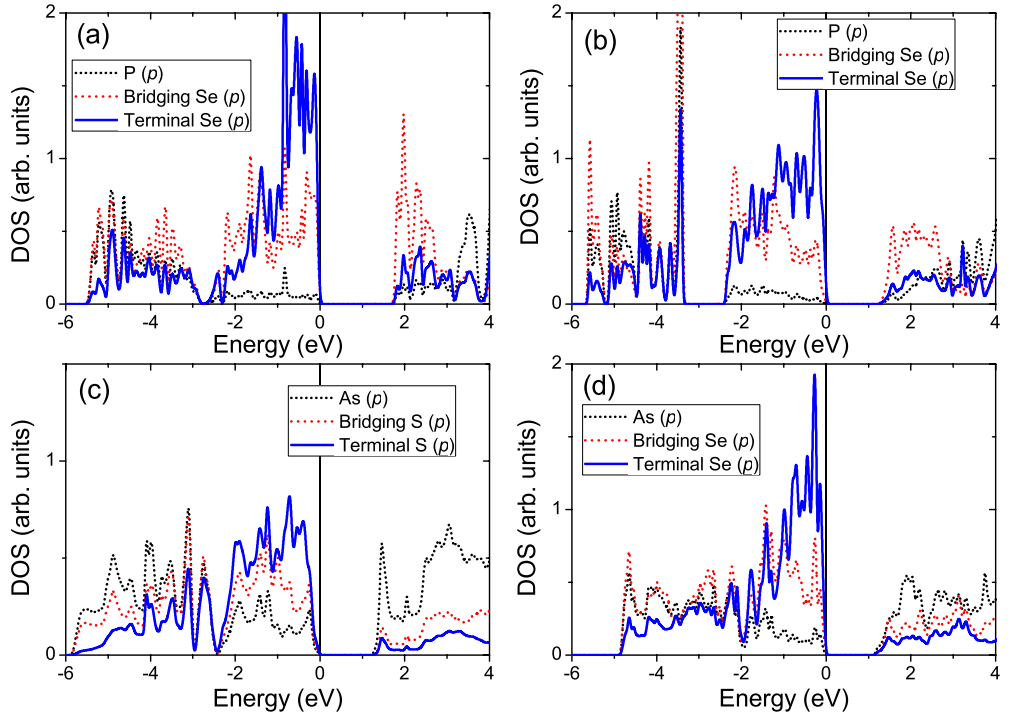

FIG. 2. (Color online) Angular-momentum-resolved local densities of states for (a) $KPSe_6$, (b) $K_2P_2Se_6$, (c) $LiAsS_2$, and (d) $NaAsSe_2$. The scissor operator is not used in these results. See text.

TABLE I. Experimental band gaps and calculated static $\chi^{(2)}$ coefficients for $KPSe_6$, $RbPSe_6$, $K_2P_2Se_6$, $LiAsS_2$, $NaAsSe_2$, GaAs, GaP, and $AgGaSe_2$. The highest static value for each material is highlighted by bold characters. ΔE_g indicates the energy difference shifted by the scissor operator.

Materials	E_g (eV)	ΔE_g (eV)	$\chi^{(2)}$ (pm/V)
$KPSe_6$	2.16[a]	0.42	$\chi^{(2)}_{131}=-39.0$, $\chi^{(2)}_{223}=-35.8$, $\chi^{(2)}_{333}=\mathbf{151.3}$
$RbPSe_6$	2.18[a]	0.40	$\chi^{(2)}_{131}=-39.9$, $\chi^{(2)}_{223}=-22.7$, $\chi^{(2)}_{333}=\mathbf{149.4}$
$K_2P_2Se_6$	2.09[b]	0.88	$\chi^{(2)}_{122}=\mathbf{53.7}$
$LiAsS_2$	1.60[c]	0.64	$\chi^{(2)}_{111}=-91.9$, $\chi^{(2)}_{122}=-25.7$, $\chi^{(2)}_{133}=-107.7$ $\chi^{(2)}_{131}=65.7$, $\chi^{(2)}_{223}=-4.1$, $\chi^{(2)}_{333}=\mathbf{196.3}$
$NaAsSe_2$	1.75[d]	0.69	$\chi^{(2)}_{111}=3.2$, $\chi^{(2)}_{122}=18.3$, $\chi^{(2)}_{133}=18.9$ $\chi^{(2)}_{131}=31.5$, $\chi^{(2)}_{223}=19.9$, $\chi^{(2)}_{333}=\mathbf{324.6}$
GaAs	1.52	0.93	$\chi^{(2)}_{123}=\mathbf{181.6}$
GaP	2.32	0.72	$\chi^{(2)}_{123}=\mathbf{95.3}$
$AgGaSe_2$	1.8	1.46	$\chi^{(2)}_{333}=\mathbf{64.7}$

[a]Reference 6.
[b]Reference 7.
[c]Reference 8.
[d]Reference 9.

$AgGaSe_2$ have only one nonzero $\chi^{(2)}$ component in the static limit. The $\chi^{(2)}$ calculations for $RbPSe_6$ illustrate the effect of alkali-metal atoms on the electronic structures of these materials: $RbPSe_6$ shows nearly the same $\chi^{(2)}$ results as $KPSe_6$ since both are isostructural (same space group $Pca2_1$), and their lattice-constant difference is less than 2.5%. The calculated static results for GaAs, GaP, and $AgGaSe_2$ are in good agreement with previous theoretical and experimental studies, 172–180, 74–82, and 64–68 pm/V, respectively.[2,18]

As a result of the small band gaps of these chalcogenides compared to oxides such as LiB_3O_5, the near-infrared and midinfrared photon energy ranges are of most importance for SHG applications. Therefore, the static $\chi^{(2)}$ values for these materials are very important and can be used to estimate their relative SHG efficiency. This is based on the fact that $\chi^{(2)}$ values slowly increase up to half the band gap as shown in Fig. 3, since 2ω resonances begin near half the band gap[2,20] due to $E-2\omega$ terms in the denominator of the frequency-dependent formulas.[16] The maximum resonances in the $\chi^{(2)}$ spectra of these materials are between 1.0 and 2.5 eV in Fig. 3 and have a proportional correlation with the static limits due to the KKR.

Unlike for linear response, it is difficult in general to find the band-structure origins of the second-harmonic susceptibilities due to multiple resonances and possible sign changes in the matrix-element products.[2] However, for low photon energies, we find that all band gaps, band dispersions near the band-gap region, and optical matrix elements are of great importance in determining the magnitude of the $\chi^{(2)}$ values. In particular, only a small energy window near the band gap dominates the $\chi^{(2)}$ values including the static limit due to 2ω resonances near half band gap.[2] In general, smaller band gaps yield larger $\chi^{(2)}$ values due to the smaller energy differences in the denominator, but only if the electronic structures are not significantly changed. As shown in Table I, the band gap, in fact, is not a decisive factor for $\chi^{(2)}$ values of $KPSe_6$, $K_2P_2Se_6$, $LiAsS_2$, and $NaAsSe_2$, and thus a detailed analysis of their electronic structures is required.

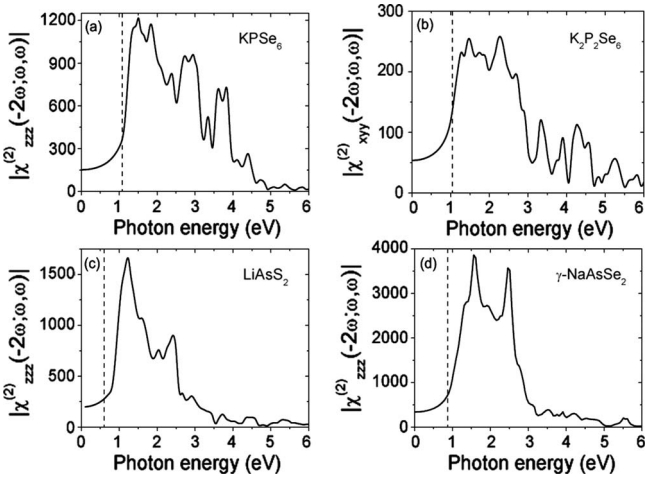

FIG. 3. Frequency-dependent SHG coefficients (pm/V) for (a) $KPSe_6$, (b) $K_2P_2Se_6$, (c) $LiAsS_2$, and (d) $NaAsSe_2$. The vertical dashed lines indicate the energy at half the band gap for each material.

Although the alkali-metal chalcogenides studied here have common DOS features, the band structures (Fig. 4) and joint density of states (JDOS) (Fig. 5) in $KPSe_6$ and $K_2P_2Se_6$ illustrate that the differences in $\chi^{(2)}$ values between these materials are caused by their electronic structural differences. The relatively more dispersed bands near the conduction-band minimum (CBM) in $K_2P_2Se_6$ produce the small and slowly increasing JDOS near the band gap compared to $KPSe_6$, as in Figs. 4 and 5(a). These materials have the same constituent atoms, P and Se, in the chains and thus are not expected to have significantly different optical matrix elements—a behavior best illustrated in Fig. 5(b). While Fig. 3 shows the true frequency-dependent SHG coefficients calculated with the real optical matrix elements, the model hypothetical SHG coefficients are calculated for analysis, as in Fig. 5(b), under the condition that all the optical matrix elements have the same constant value, 0.01, which then directly reflects the effect of the JDOS on the $\chi^{(2)}$ results.[2] The hypothetical static limits with this condition yield 170.45 pm/V for $KPSe_6$ and 47.89 pm/V for $K_2P_2Se_6$ in Fig. 5(b), which are similar to the true values, 151.3 and 53.7 pm/V in Fig. 3, respectively.

The LDOS in Fig. 2 also shows the origin of differences between $KPSe_6$ and $K_2P_2Se_6$. The relatively weak covalent P-bridging Se interactions in $K_2P_2Se_6$, compared to P-terminal Se and P-P covalent bonds of $K_2P_2Se_6$, cause strongly localized characteristics within the $[P_2Se_6]$ units; this results in essentially flat bands and thus very sharp peaks in the LDOS [Fig. 2(b)] for the lower energy range between −6 and −2.5 eV below VBM [Figs. 4(b) and 6]. Note that P-P bondings are absent in $KPSe_6$ as shown in Fig. 1. On the other hand, the band-gap region, especially the CBM of $K_2P_2Se_6$, has relatively dispersed band characteristics compared to $KPSe_6$, which can also be verified in Fig. 2. The fact that a large number of Se neighbors (within 3.5 Å) may be

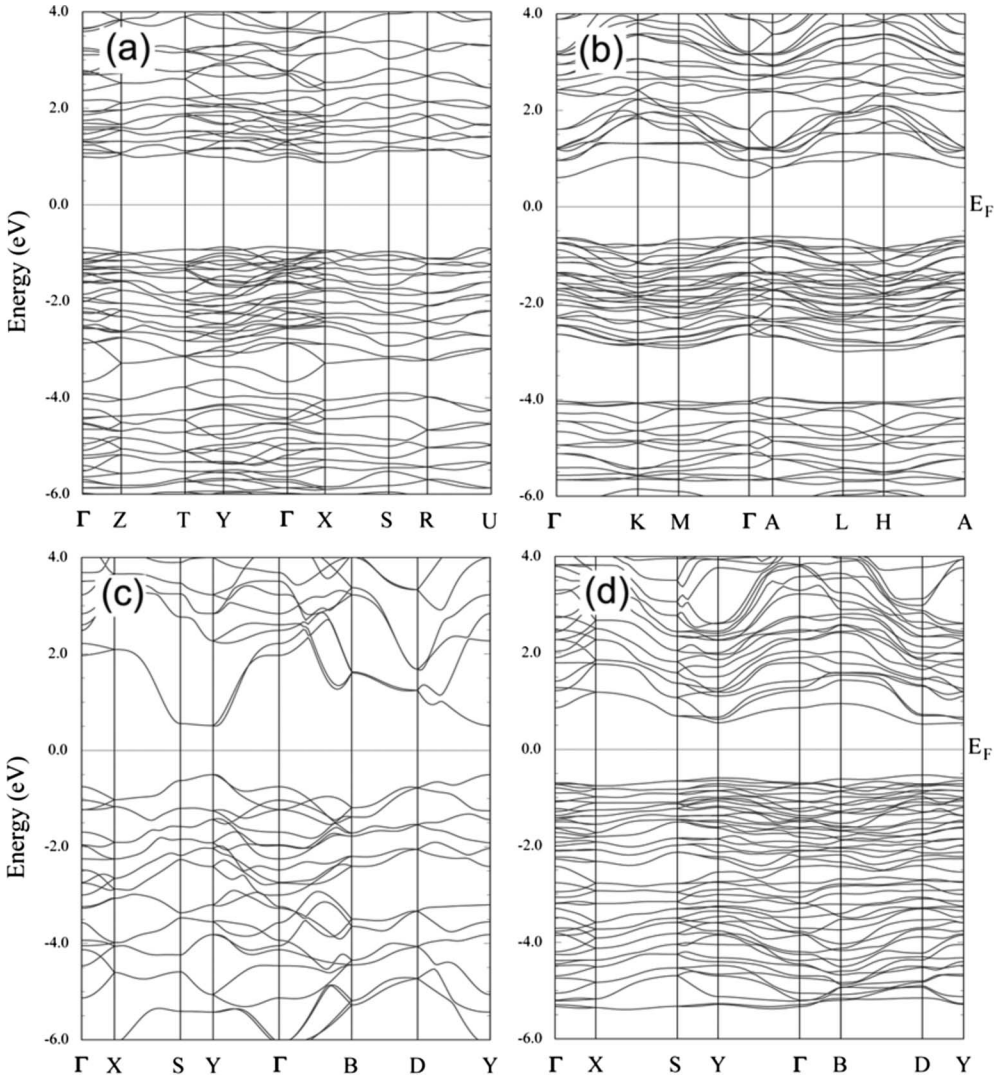

FIG. 4. Band structures for (a) $KPSe_6$, (b) $K_2P_2Se_6$, (c) $LiAsS_2$, and (d) $NaAsSe_2$.

hybridized with K *s* states in $K_2P_2Se_6$ (Fig. 7) appears to cause the delocalization of Se *p* states near the band gap compared to $KPSe_6$. These materials demonstrate the importance of crystal and electronic structures (e.g., density of states) in determining SHG coefficients.

Compared to $KPSe_6$ and $K_2P_2Se_6$, the electronic-structure calculations for $LiAsS_2$ yield greatly broadened bands [Fig. 4(c)] which are attributed to the strong interchain interactions from the small Li cations and thus to the weakening of an anisotropic one-dimensional characteristic.[8] This should result in significantly smaller JDOS near the band gap as shown in Fig. 5(a) and thus would give rise to much smaller $\chi^{(2)}$ values [25.14 pm/V in Fig. 5(b)] if the optical matrix elements are similar to those of other materials. While the smaller band gap of $LiAsS_2$ may have the effect of increasing the $\chi^{(2)}$ values, the small difference in the band gap between $LiAsS_2$ and other materials has a negligible effect, as shown in Fig. 5(b). The static $\chi^{(2)}$ value is, however, 196.3 pm/V, which is much larger than the 151.3 pm/V value of $KPSe_6$. The LDOS in Fig. 2 provides an important clue for this. The main contribution to the optical transition near the band gaps of $KPSe_6$ and $K_2P_2Se_6$ is from terminal Se to bridging Se *p* states. Interestingly, however, $LiAsS_2$ (and $NaAsSe_2$) has a significant optical transition from terminal S (and Se) to As *p* states since there is a large contribution of As *p* states in the CBM. This is due to the more extended As *p* states in their conduction bands compared to P *p* states of $KPSe_6$ and $K_2P_2Se_6$. The direct covalent bonds between terminal S (or Se) and As atoms in $LiAsS_2$ (or $NaAsSe_2$) then lead to the large spatial overlap compared to $KPSe_6$ and

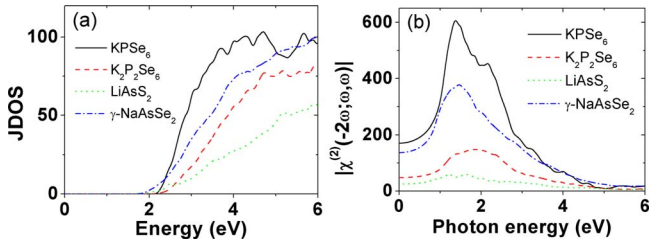

FIG. 5. (Color online) (a) Joint densities of states. (b) Model hypothetical frequency-dependent SHG coefficients (arbitrary units) when all the momentum matrix elements have the same constant value, namely, $P_{nm}=0.01$.

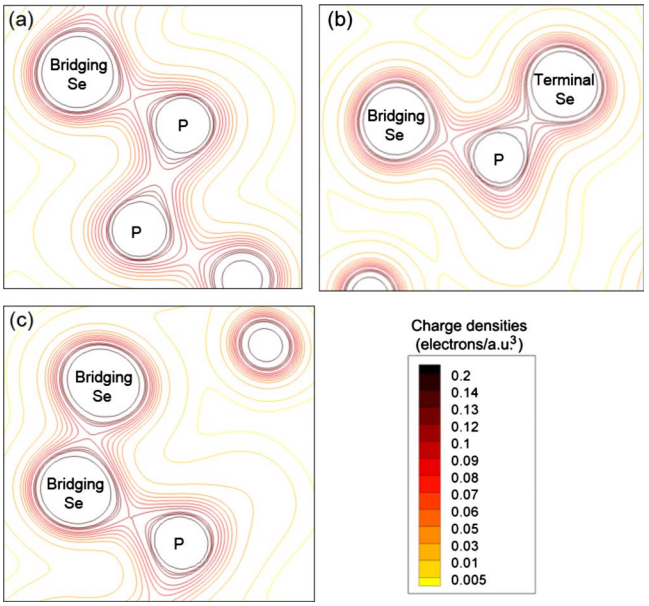

FIG. 6. (Color online) Charge densities for various bondings in $K_2P_2Se_6$ of (a) bridging Se-P-P, (b) bridging Se-P-terminal Se, and (c) bridging Se-bridging Se-P. Note that the bonding distances of P-bridging Se, P-P, and P-terminal Se are 2.331, 2.245, and 2.132 Å, respectively.

$K_2P_2Se_6$. In relation to this, it is envisioned that As, which is larger than P, provides stronger covalency and therefore larger optical matrix elements. The covalent-bonding character with the large spatial overlap of wave functions between initial and final states of optical transitions plays an important role in optical-matrix-element products[21] and therefore SHG coefficients. Indeed, due to larger optical matrix elements, GaAs has a large static $\chi^{(2)}$ value, 181.6 pm/V as shown in Table I. Furthermore, the static $\chi^{(2)}$ value of $AgGaTe_2$ is also known to be approximately twice as large as that of $AgGaSe_2$.[2]

Finally, $NaAsSe_2$ points to a good strategy in designing materials for SHG coefficients; its quasi-one-dimensional structure provides the high density of states in Fig. 2(d) and thus the large JDOS (136.77 pm/V calculated with the hypothetical $\chi^{(2)}$ calculations) in the band-gap region in Fig. 5(a), like those of $KPSe_6$ and $K_2P_2Se_6$. In addition to the benefit of the large JDOS, the large spatial overlap between optical transition states yields a large static true $\chi^{(2)}$ value of $NaAsSe_2$, 324.6 pm/V, as calculated in Fig. 3. It is approximately five times larger than the static SHG coefficient of $AgGaSe_2$, a commercially used material. This is a very high value as compared to materials with band gap larger than 1.0 eV.

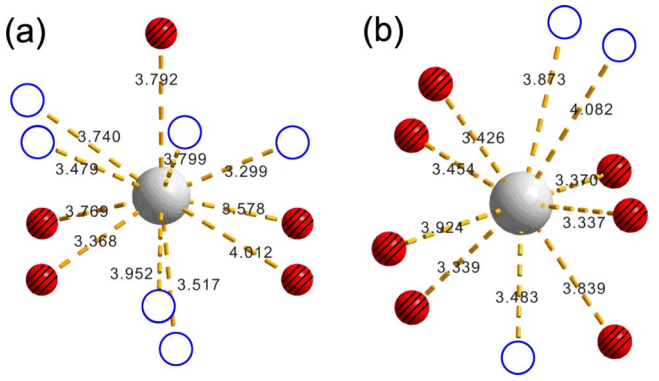

FIG. 7. (Color online) Immediate coordination environment of K atoms in (a) $KPSe_6$ and (b) $K_2P_2Se_6$. Gray large spheres represent K atoms. Small empty spheres are bridging Se atoms. Small shaded spheres are terminal Se atoms. Distances between K and Se atoms are given. Note that there are three and six Se neighbors around K within 3.5 Å in (a) $KPSe_6$ and (b) $K_2P_2Se_6$, respectively.

IV. CONCLUSIONS

We conclude that it is a quasi-one-dimensional crystal structure with a strong covalent character that yields very large second-harmonic susceptibilities and thus extremely strong SHG intensities. This work not only explains the physical reasons for their large second-harmonic susceptibilities but also opens a way of thinking in the design of better SHG materials that involves the manipulation of the electronic structures of low-dimensional crystals with different compositions, or with atom substitutions, to achieve more delocalized atomic bonds.

ACKNOWLEDGMENTS

This work was supported by NSF through its MRSEC program at the Materials Research Center of Northwestern University under Grant No. DMR 0520513. We are grateful to Jun Li and Rolando Saniz for helpful discussions.

[1] C. Chen, Y. Wang, B. Wu, K. Wu, W. Zeng, and L. Yu, Nature (London) **373**, 322 (1995).
[2] S. N. Rashkeev and W. R. L. Lambrecht, Phys. Rev. B **63**, 165212 (2001).
[3] P. G. Schunemann, Proc. SPIE **6455**, 64550R (2007).
[4] D. N. Nikogosyan, *Nonlinear Optical Crystals: A Complete Survey* (Springer-Science, New York, 2005).
[5] M. Baudrier-Raybaut, R. Haïdar, Ph. Kupecek, Ph. Lemasson, and E. Rosencher, Nature (London) **432**, 374 (2004).
[6] I. Chung, J. Do, C. G. Canlas, D. P. Weliky, and M. G. Kanatzidis, Inorg. Chem. **43**, 2762 (2004).
[7] I. Chung, C. D. Malliakas, J. I. Jang, C. G. Canlas, D. P. Weliky, and M. G. Kanatzidis, J. Am. Chem. Soc. **129**, 14996 (2007).
[8] T. K. Bera, J.-H. Song, A. J. Freeman, J. I. Jang, J. B. Ketterson, and M. G. Kanatzidis, Angew. Chem., Int. Ed. **47**, 7828 (2008).
[9] T. K. Bera (private communication).
[10] E. Wimmer, H. Krakauer, M. Weinert, and A. J. Freeman, Phys. Rev. B **24**, 864 (1981).
[11] H. J. F. Jansen and A. J. Freeman, Phys. Rev. B **30**, 561 (1984).
[12] L. Hedin and B. Lundqvist, J. Phys. C **4**, 2064 (1971).
[13] J. E. Sipe and E. Ghahramani, Phys. Rev. B **48**, 11705 (1993).
[14] C. Aversa and J. E. Sipe, Phys. Rev. B **52**, 14636 (1995).

[15] J. L. P. Hughes and J. E. Sipe, Phys. Rev. B **53**, 10751 (1996).
[16] S. N. Rashkeev, W. R. L. Lambrecht, and B. Segall, Phys. Rev. B **57**, 3905 (1998).
[17] W. R. L. Lambrecht and S. N. Rashkeev, Phys. Status Solidi B **217**, 599, (2000).
[18] F. Nastos, B. Olejnik, K. Schwarz, and J. E. Sipe, Phys. Rev. B **72**, 045223 (2005).
[19] D. A. Kleinman, Phys. Rev. **126**, 1977 (1962).
[20] C. G. Duan, J. Li, Z. Q. Gu, and D. S. Wang, Phys. Rev. B **59**, 369 (1999).
[21] J. Ingers, K. Maschke, and S. Proennecke, Phys. Rev. B **37**, 6105 (1988).